

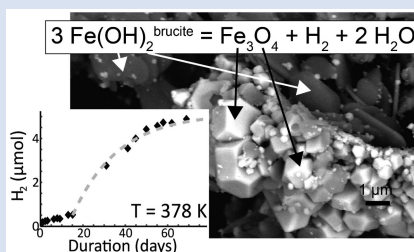
Kinetics of low-temperature H₂ production in ultramafic rocks by ferroan brucite oxidation

W. Carlin^{1,2}, B. Malvoisin^{1*}, F. Brunet¹, B. Lanson¹, N. Findling¹, M. Lanson¹,
T. Fargetton², L. Jeannin², O. Lhote²



<https://doi.org/10.7185/geochemlet.2408>

Abstract



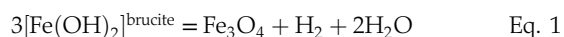
Ferroan brucite, (Mg,Fe)(OH)₂, is among the potential mineral candidates for low temperature (<423 K) abiotic H₂ production in ultramafic rocks. To verify this assumption, synthetic ferroan brucite with grain size similar to that observed in natural samples (40–100 nm) was reacted with pure water at temperatures ranging from 348 to 573 K. Experimental products are consistent with the reaction $3 \text{Fe}(\text{OH})_2^{\text{brucite}} = \text{Fe}_3\text{O}_4 + \text{H}_2 + 2 \text{H}_2\text{O}$. This reaction reached completion in ~2 months at 378 K and is thermally activated with an activation energy of 145 ± 1 kJ/mol. The standard state formation enthalpy and the third law entropy of amakinite, Fe(OH)₂, were refined from the experimental dataset. The new thermodynamic parameters imply that ferroan brucite is stable at significantly lower hydrogen activity than previously calculated. The alteration of Fe-brucite produces H₂ at rates compatible with present day observations of H₂ emissions in natural settings (ophiolite and mid-oceanic ridges). However, efficient fluid renewal is required, as opposed to H₂ production through olivine serpentinisation, which can proceed in static hydraulic conditions.

Received 9 October 2023 | Accepted 24 January 2024 | Published 5 March 2024

Introduction

Hydrothermal circulation across upper mantle rocks at mid-ocean ridges promotes serpentinisation reactions. In the course of these reactions, olivine reacts with water to form serpentine, magnetite and ferroan brucite, (Mg,Fe)(OH)₂, along with abiotic hydrogen (Moody, 1976). As observed in ophiolites (Neal and Stanger, 1983; Abrajano *et al.*, 1990; Leong *et al.*, 2023), ultramafic rocks can still produce H₂ at low temperature (*i.e.* at $T < 423$ K), even if they are extensively serpentinised. The extrapolation of experimental kinetic data collected in the 473–623 K range (*e.g.*, McCollom *et al.*, 2016) indicates that serpentinisation of olivine with a grain size of 500 μm should reach a reaction progress above 90 % in at least 10,000 yr at temperatures below 423 K.

The serpentinisation of olivine produces secondary minerals, including ferroan brucite, which are Fe²⁺-rich and which can further react to produce H₂ + magnetite at low temperature:



where $[\text{Fe}(\text{OH})_2]^{\text{brucite}}$ represents the Fe component of ferroan brucite.

Petrographic data on ophiolite and dredge seafloor samples (Jöns *et al.*, 2017; Klein *et al.*, 2020; Ellison *et al.*, 2021) seem to indicate that Reaction 1 could proceed at sub-surface conditions in partly serpentinised ultramafic rocks. H₂ production was achieved in hydrothermal experiments carried out

on serpentinised peridotite at 373 K and was attributed to magnetite formation at the expense of ferroan brucite (Miller *et al.*, 2017).

In order to test the potential of Reaction 1 to produce H₂ at temperatures below 423 K in ultramafic rocks, the kinetics and thermodynamics of Reaction 1 were investigated experimentally here using synthetic (Mg_{1-x}Fe_x)(OH)₂ of grain size (40–100 nm) and composition (x from 0.156 to 0.205) relevant to natural ferroan brucite (Malvoisin *et al.*, 2020).

Materials and Methods

Ferroan brucite (Mg_{1-x}Fe_x)(OH)₂, with x ranging from 0.156 to 0.205, was synthesised under ambient conditions from a stoichiometric solution of dissolved Fe(II) and Mg chlorides, as described in Carlin *et al.* (2023). The ferroan brucite obtained by this method formed platelets 40 to 100 nm across (Fig. 1a). It was loaded under an Ar atmosphere with degassed ultrapure water either in welded shut gold capsules ('caps' experiments) or in 50 mL Parr 5500 series titanium reactors ('SP' experiments; see details in Tables S-2 and S-3). The capsules were run either in horizontal cold seal pressure vessels at temperatures from 348 to 573 K at 20 MPa (caps#1 to #15) or in an oven at temperatures of 378 and 423 K at the liquid-vapour equilibrium pressure (P_{sat} , caps#t1 to #t12). Titanium reactor experiments, SP#3 to SP#5, were conducted in the 423 to 473 K range, also at P_{sat} . SP#6 was run at 378 K with an initial Ar pressure of ~5 MPa.

1. Université Grenoble Alpes, USMB, CNRS, IRD, UGE, ISTerre, France

2. Storengy, ENGIE, France

* Corresponding author (email: benjamin.malvoisin@univ-grenoble-alpes.fr)



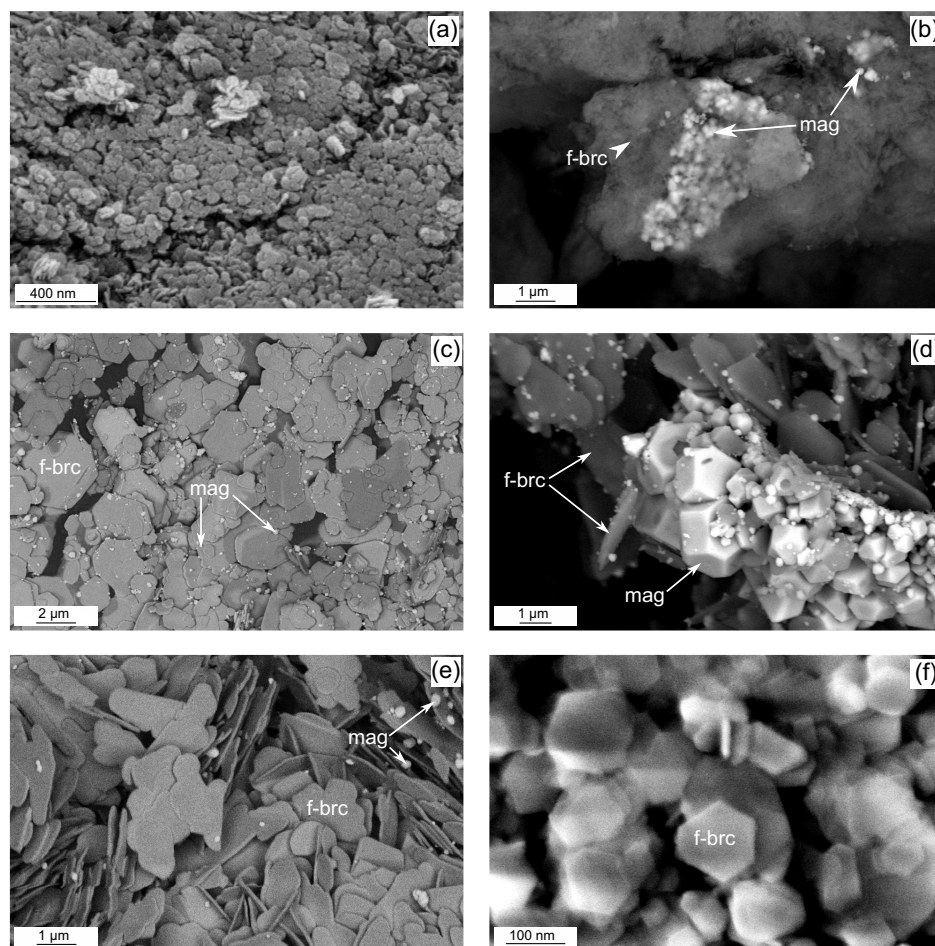


Figure 1 Back-scattered images of (a) the starting ferroan brucite and (b–f) its reaction products. (b) Caps#9; 378 K, 2.5 days. (c, d) SP#3; 473 K, 8 days. Euhedral micrometre-sized magnetite is visible. (e) Caps#15; 573 K, 2 days. Note that ferroan brucite platelets have recrystallised. (f) SP#6; 378 K, 69 days. ~100 nm wide euhedral ferroan brucite platelets are observed. f-brc, ferroan brucite; mag, magnetite.

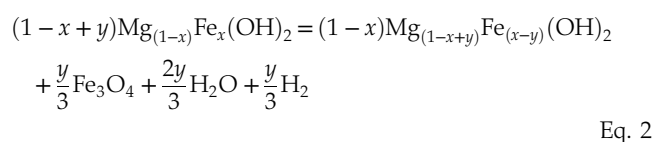
Pressure evolution in SP experiments was monitored at ± 2 kPa with a Keller pressure sensor PA-33X. After the experiments, the H_2 produced and trapped in the gold capsule was sampled using the protocol described in Malvoisin *et al.* (2013) and analysed by gas chromatography. H_2 leakage through the gold capsule walls is negligible at the temperatures investigated here (Malvoisin *et al.*, 2013). The amount of H_2 produced in titanium reactors was quantified either on the gas sampled at the run conditions, and/or at the end of the experiment. No H_2 was detected in two blank experiments performed at 378 and 473 K over more than 40 days with capsules containing only degassed ultrapure water (100 μ L). Before experiments, the titanium reactors were heated to 523 K during one day in air to extract any H_2 potentially solubilised in the reactor wall (Louthan and Derrick, 1975), and to ensure Ti surface oxidation prior to reaction. No hydrogen production was detected in these blank experiments. Details of the sample characterisation techniques are provided in the Supplementary Information.

Results and Discussion

Ferroan brucite oxidation reaction. In all experiments, ferroan brucite partly decomposed into magnetite + H_2 (Table S-2). The H_2 yield increased from 4×10^{-3} to 220 μ mol of H_2 per gram of starting material when the temperature increased from 348 to 573 K. In eight experiments (Table S-2), pyroaurite was detected (<20 wt. %), indicating the presence of minor CO_2 in the reacting

medium. Pyroaurite does not involve significant H_2 production (Carlin *et al.*, 2023). Its impact on H_2 production rate is, thus, mainly associated with the lowering of the amount of ferroan brucite available for H_2 production. However, for experiments used for determining kinetic and thermodynamic parameters, we estimated that a maximum of 3.4 wt. % of the initial ferroan brucite was consumed to form pyroaurite. This leads to an error on the H_2 production rate that is small compared to the error associated with H_2 measurement of ~11 %. The Fe content ($X_{Fe(OH)_2}$) of ferroan brucite was determined from the refined unit cell parameters (Table S-2) based on Vegard's law (Carlin *et al.*, 2023). It was found to vary from 0.1 to 0.2, *i.e.* equal or slightly below $X_{Fe(OH)_2}$ in the ferroan brucite starting material. Recrystallisation of ferroan brucite as platelets was observed in the highest temperature experiments (Fig. 1). Unless metastable growth occurred, this observation suggests that ferroan brucite with $X_{Fe(OH)_2} < 0.2$ is a stable reaction product in these experiments.

Altogether, the experimental results revealed that brucite partly reacted during the experiments according to Reaction 1, leading to the overall reaction:



Eq. 2

where x is the initial $X_{\text{Fe}(\text{OH})_2}$ and y is a parameter related to reaction progress such as $0 \leq y \leq x$, which reflects that only a fraction, y/x , of the $\text{Fe}(\text{OH})_2$ component in ferroan brucite has reacted. Indeed, thermodynamic equilibrium may well be achieved for $y < x$.

H_2 production rate and brucite oxidation rate. The amount of produced H_2 was used to retrieve the progress of Reaction 2. Magnetite was not used to infer reaction progress because, due to the presence of minor Fe^{3+} in the starting material, part of the magnetite product may form independently of Reaction 2, i.e. without H_2 production (Carlin *et al.*, 2023). The amount of H_2 produced in the SP experiments did not induce pressure changes significant enough to retrieve isothermal H_2 -production rate laws directly from pressure monitoring. However, the qualitative pressure evolution was used to determine the overall duration of the H_2 production stage, which, in turn, was used to model the reaction kinetics (see Supplementary Information for details). H_2 production kinetics at 378 K could be accurately retrieved from Run SP#6, where gas was regularly sampled (Fig. 2a). In addition, a series of experiments in gold capsules (caps#t5 to #t12) were stopped after different durations and H_2 was analysed in order to further constrain the kinetics of Reaction 2 (Fig. 2b). These experimental data were fitted to a kinetic law (Lasaga, 1998; see Supplementary Information for details) with the reaction rate (r) as:

$$r = r_0 \times \left(1 - \frac{Q}{K}\right) \quad \text{Eq. 3}$$

where $r_0 = k_0 \times A \times \exp\left(\frac{-E_a}{RT}\right)$ with k_0 a kinetic constant, A the $\text{Fe}(\text{OH})_2$ specific surface area, E_a the activation energy, R the gas constant and T the temperature. Q and K are the reaction quotient and the equilibrium constant of Reaction 1, respectively. The standard state is defined here with unit activity for pure minerals and water at any temperature and pressure, as well as unit fugacity for ideal gas at 1 bar of pressure and any temperature. Q was approximated to $\frac{P_{\text{H}_2}}{X_{\text{Fe}(\text{OH})_2}}$ with P_{H_2} the H_2 partial pressure at the conditions of the experiment and $X_{\text{Fe}(\text{OH})_2}$ the molar fraction of $\text{Fe}(\text{OH})_2$ in ferroan brucite, by assuming ideal behaviour for H_2 and $\text{Fe}(\text{OH})_2$ in the gas phase and in the brucite solid-solution, respectively. $X_{\text{Fe}(\text{OH})_2}$ was calculated from Equation 2, based on the number of moles of produced H_2 (n_{H_2}). P_{H_2} was derived from n_{H_2} considering the amount of H_2 dissolved in the solution as calculated using PHREEQC (Parkhurst and Appelo, 2013). K was estimated with the same procedure as Q , by considering that equilibrium H_2 pressure equals the H_2 partial pressure in the gas at the last measurement multiplied by a factor, λ , slightly above 1 (see Supplementary Information for details on this factor). Fitted r_0 values are displayed in Figure 2c as a function of reciprocal temperature. The slope in the linear fit corresponds to an activation energy of 145 ± 1 kJ/mol. The intercept of the fit provides a $k_0 \times A$ quotient of 8.97×10^7 mol s⁻¹ g⁻¹.

Experimental constraints on thermodynamic properties of ferroan brucite. Based on the kinetic law derived in the previous section, 17 experiments reached equilibrium (Table S-2). These experiments were, thus, used to constrain the equilibrium constant (K) of Reaction 1.

As discussed above, a set of K values can be calculated based on n_{H_2} , measured at the end of each experiment. A pair of $\Delta_f H^\circ$ and S° values for the $\text{Fe}(\text{OH})_2$ end member was retrieved by least square regression through this set of K values (see Supplementary Information for thermodynamic calculation details). $\Delta_f H^\circ_{\text{Fe}(\text{OH})_2}$ and $S^\circ_{\text{Fe}(\text{OH})_2}$ of -581.3 ± 2.9 kJ/mol and

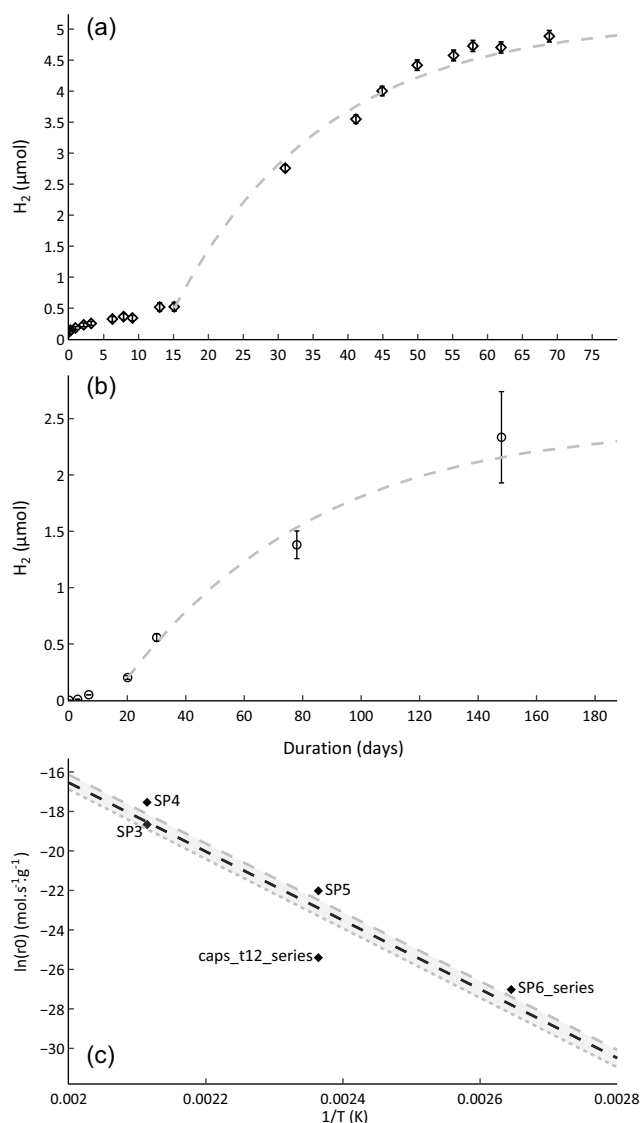


Figure 2 Kinetics of ferroan brucite alteration. (a) Number of moles of produced H_2 as a function of time at 378 K (Run SP#6; black diamonds). (b) Number of moles of produced H_2 as a function of time at 423 K (Runs caps#t5 to caps#t12; black circles). The dashed lines in (a) and (b) correspond to a fit of the data with Equation 3. (c) $\ln(r_0)$ vs. $1/T$. The linear regression of r_0 is displayed with a black dashed line ($R^2 = 0.87$) and the grey dashed lines are linear regressions for r_0 with λ values of 1.01 and 1.20.

86.4 ± 6.3 J/mol/K were obtained, respectively. These thermodynamic values are only relevant for calculations using the same standard states as those used here, as well as the same assumption of unit activity and fugacity coefficients for ferroan brucite solid solution and H_2 in the gas phase, respectively. They fall in the range of published values for $\text{Fe}(\text{OH})_2$ (Table S-4, Fig. S-3). The $\Delta_f H^\circ_{\text{Fe}(\text{OH})_2}$ value is consistent with the value by Ziemniak *et al.* (1995) and departs by 1.2 % from $\Delta_f H^\circ_{\text{Fe}(\text{OH})_2}$, tabulated in the NIST-JANAF database (Chase, 1998). The values of the NIST-JANAF database only differ by 0.1 % from those commonly used for thermodynamic modelling of fluid-rock interactions in ultramafic rocks (McCollom and Bach, 2009). H_2 production prediction for our experiments is overestimated by more than one order of magnitude with the McCollom and Bach's (2009) database (Fig. S-4).

Implications for low-T H_2 production in ultramafic systems. Olivine serpentinisation (e.g., McCollom *et al.*, 2016)

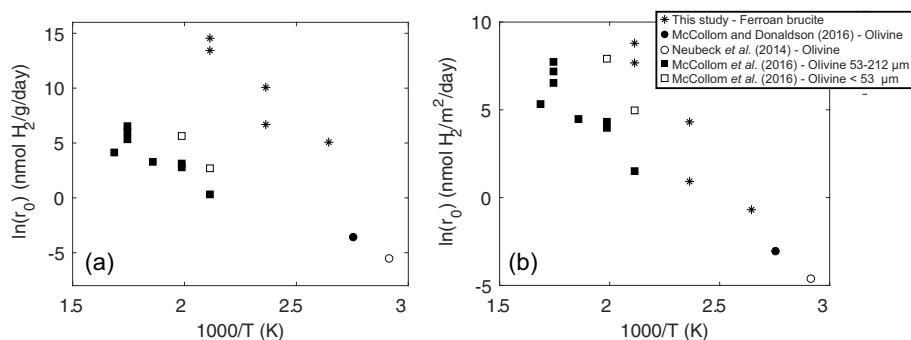


Figure 3 Comparison of experimentally determined rate of H₂ production for ferroan brucite (r_0 , this study) and olivine serpentinisation (Neubeck *et al.*, 2014; McCollom and Donaldson, 2016; McCollom *et al.*, 2016). (a) Reaction rate *per mass* of starting material (r_0). (b) Reaction rate *per reactive surface area* (r_0/A) with A the specific surface area either measured with the BET method or calculated with the relationship provided in Brantley and Mellott (2000).

and ferroan brucite alteration (Miller *et al.*, 2017; Ellison *et al.*, 2021) are the two main processes that have been proposed to account for H₂ production at low temperature ($T < 423$ K) in ultramafic rocks. Excluding kinetic experiments interpreted as being distorted by artefacts (McCollom and Donaldson, 2016), a maximum of 0.028 nmol H₂/g olivine/day was proposed for H₂ production by olivine serpentinisation at 363 K (Fig. 3a). In comparison, the rate of H₂ production measured here during ferroan brucite reaction (r_0) is approximately three orders of magnitude higher (Fig. 3a). When weighted by the specific surface area of the powders used in the various experiments, however, the reaction rates are rather well aligned in an Arrhenius plot with an activation energy of ~ 81 kJ/mol (Fig. 3b). The difference in grain sizes between olivine used in the experiments depicted in Figure 3 (38–212 μm) and the synthetic ferroan brucite used here (~ 50 nm) probably plays a key role in their difference of reactivity.

The respective contribution of olivine and Fe-brucite alteration to the H₂ production rate in natural systems was evaluated using a numerical approach. A fluid–serpentinised dunite system composed of olivine (grain size of 500 μm; Malvoisin *et al.*, 2017), ferroan brucite (grain size of 50 nm; Malvoisin *et al.*, 2021) and water was modelled with H₂ being only produced by alteration of the latter minerals. A range of escape rates of H₂ (advection and/or diffusion) was defined in order to simulate hydrothermal activity at mid-ocean ridges, water infiltration in an ophiolitic unit or sub-stagnant hydraulic conditions in a deep aquifer. The temperature was set to 363 K, relevant to low- T serpentinisation (Fig. 4; see model details in Supplementary Information).

The model shows that ferroan brucite is the first mineral to react with a rate that is three orders of magnitude faster than that of olivine, leading to a rapid H₂ production in the first year of the reaction (Fig. 4b). In a closed system, ferroan brucite reaction rapidly stops due to the attainment of thermodynamic equilibrium ($Q/K = 1$). The adjustment of the thermodynamic parameters of Fe(OH)₂ proposed here (1.8 % and 1.2 % for $S^\circ_{\text{Fe(OH)}_2}$ and $\Delta_f H^\circ_{\text{Fe(OH)}_2}$, respectively, compared to the database of McCollom and Bach, 2009) has a strong impact on the predicted equilibrium H₂ partial pressure and, thus, on the amount of H₂ that is produced. At 363 K, equilibrium is achieved for a H₂ molality of 2.2×10^{-5} mol/kg, while it is two orders of magnitude higher (5.0×10^{-3} mol/kg) with the database of McCollom and Bach (2009). At 313 K, a difference of three orders of magnitude for H₂ molality between the two database is predicted. The oxygen fugacity (f_{O_2}) lies on the H₂O/H₂(g) equilibrium with the database of McCollom and Bach (2009) and five orders of magnitude above with the thermodynamic data derived here. Interestingly, this latter f_{O_2} is consistent with the f_{O_2} measured at the bottom of Holes BA1A, BA1D and BA4A during the Oman Drilling Project (Kelemen *et al.*, 2021). After ferroan brucite reaction, olivine completely reacts in the model in approximately 3 Myr and ultimately produces 3000 times more H₂ than ferroan brucite (Fig. 4a).

Ferroan brucite can further react if, at the same time, H₂ escapes from the system at a rate exceeding that of H₂ production associated with olivine serpentinisation (Fig. 4c). This corresponds to minimum H₂ escape rates of 10^{-5} and 7×10^{-4} mol H₂/day/kg rock at 313 and 363 K, respectively. The estimated

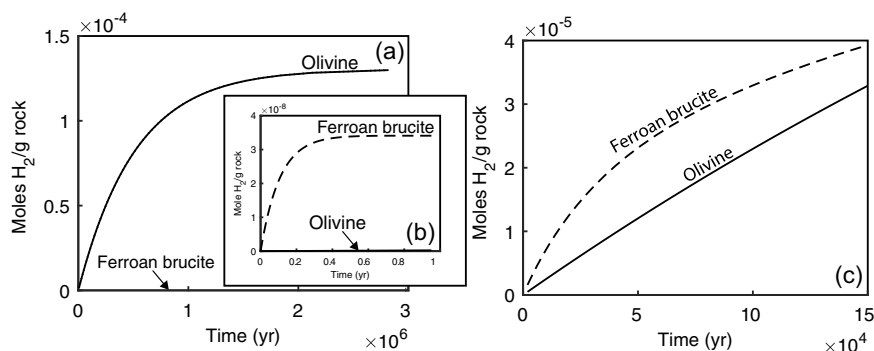


Figure 4 Numerical modelling of the contribution of ferroan brucite alteration and olivine serpentinisation to H₂ production as a function of time in a partly altered peridotite (see Supplementary Information for details). (a) General view and (b) incipient stage simulation in a closed system (no H₂ leak associated with diffusion or fluid advection). (c) Simulation by considering advection of a fluid at a rate of 1.4×10^{-4} kg water/day/kg rock. Dashed line: H₂ production associated with ferroan brucite alteration. Solid line: H₂ production associated with olivine serpentinisation.

maximum escape rate by vertical diffusion is three orders of magnitude lower than this threshold value (see [Supplementary Information](#) for details), suggesting that vertical diffusion is not sufficient to drive ferroan brucite reaction. The threshold value is achieved by water renewal at a minimum rate of 7×10^{-6} and 3×10^{-5} kg water/day/kg rock at 313 and 363 K, respectively. The average water-to-rock ratio at mid-ocean ridges is ~ 1 (Coogan *et al.*, 2019). Considering hydrothermal activity and fluid flow during a minimum of 30,000 yr (Früh-Green *et al.*, 2003), it can be converted into a mean water flux of 10^{-7} kg water/day/kg rock. In the Oman ophiolite, ferroan brucite with $x = 0.28$ can represent ~ 50 mol % of the serpentinisation reaction products (Malvoisin *et al.*, 2020). Present day alteration of such ferroan brucite may occur during interaction with rain-water. H_2 -rich hyperalkaline fluids are found at depths > 50 m (Leong *et al.*, 2023), and the recharge rate of the aquifer in Oman is 18 mm/year (Dewandel *et al.*, 2005). Combining these values leads to a mean meteoritic water flux of 3×10^{-7} kg water/day/kg rock. Both in ophiolites and on the seafloor, mean water flux estimates are, thus, approximately one order of magnitude lower than the minimum flux necessary to drive ferroan brucite reaction. However, fluid flow in ultramafic rocks is concentrated in cracks and microcracks (Dewandel *et al.*, 2005; Corre *et al.*, 2023) and is, thus, expected to be, locally, several orders of magnitude higher than the mean water flux. For example, the highest water-to-rock ratio values reported in abyssal peridotites are above 10^5 (Snow and Reisberg, 1995; Delacour *et al.*, 2008), corresponding to water fluxes $> 10^{-2}$ kg water/day/kg rock compatible with H_2 production associated with ferroan brucite oxidation. The measured maximum H_2 production rate in the Oman ophiolite is of 71,000 mol H_2 /yr for a minimal volume of altered rock of 0.05 km³ (Leong *et al.*, 2023). This corresponds to a specific flux of 10^{-3} nmol H_2 /g rock/day which is consistent with the specific H_2 production rate of 5×10^{-3} nmol H_2 /g rock/day, estimated at 313 K based on the extrapolation of the data acquired here for ferroan brucite alteration (Fig. 3). Actually, the same extrapolation for serpentinisation of olivine having a grain size of 500 μ m (Fig. 3b) yields a much lower production rate of 10^{-5} nmol H_2 /g rock/day at 313 K. Ferroan brucite oxidation could thus be a main contributor to H_2 production at temperatures below 423 K in ophiolites and on the seafloor. This is consistent with petrographic observations in natural samples showing ferroan brucite oxidation to form magnetite in open systems conditions (Bach *et al.*, 2006; Jöns *et al.*, 2017).

Acknowledgements

This work is part of a CIFRE PhD (n°2019.1672) funded by ENGIE, and performed in collaboration with Storengy. Analyses have been performed at the *Geochemistry & Mineralogy* platform of ISTERre (Université Grenoble Alpes, France). The editor, E.H. Oelkers, and two anonymous reviewers are thanked for their insightful comments and careful reading.

Editor: Eric Oelkers

Additional Information

Supplementary Information accompanies this letter at <https://www.geochemicalperspectivesletters.org/article2408>.



© 2024 The Authors. This work is distributed under the Creative Commons Attribution Non-Commercial No-Derivatives 4.0

License, which permits unrestricted distribution provided the

original author and source are credited. The material may not be adapted (remixed, transformed or built upon) or used for commercial purposes without written permission from the author. Additional information is available at <https://www.geochemicalperspectivesletters.org/copyright-and-permissions>.

Cite this letter as: Carlin, W., Malvoisin, B., Brunet, F., Lanson, B., Findling, N., Lanson, M., Fargetton, T., Jeannin, L., Lhote, O. (2024) Kinetics of low-temperature H_2 production in ultramafic rocks by ferroan brucite oxidation. *Geochem. Persp. Let.* 29, 27–32. <https://doi.org/10.7185/geochemlet.2408>

References

- ABRAJANO, T.A., STURCHIO, N.C., KENNEDY, B.M., LYON, G.L., MUEHLENBACHS, K., BOHLKE, J.K. (1990) Geochemistry of reduced gas related to serpentinization of the Zambales ophiolite, Philippines. *Applied Geochemistry* 5, 625–630. [https://doi.org/10.1016/0883-2927\(90\)90060-1](https://doi.org/10.1016/0883-2927(90)90060-1)
- BACH, W., PAULICK, H., GARRIDO, C.J., ILDEFONSE, B., MEURER, W.P., HUMPHRIS, S.E. (2006) Unraveling the sequence of serpentinization reactions: petrography, mineral chemistry, and petrophysics of serpentinites from MAR 15°N (ODP Leg 209, Site 1274). *Geophysical Research Letters* 33, L13306. <https://doi.org/10.1029/2006GL025681>
- BRANTLEY, S.L., MELLOTT, N.P. (2000) Surface area and porosity of primary silicate minerals. *American Mineralogist* 8, 1767–1783. <https://doi.org/10.2138/am-2000-11-1220>
- CARLIN, W., MALVOISIN, B., LANSON, B., BRUNET, F., FINDLING, N., LANSON, M., MAGNIN, V., FARGETTON, T., JEANNIN, L., LHOTE, O. (2023) Fe^{III}-substituted brucite: Hydrothermal synthesis from (Mg_{0.8}Fe_{0.2})-brucite, crystal chemistry and relevance to the alteration of ultramafic rocks. *Applied Clay Science* 234, 106845. <https://doi.org/10.1016/j.clay.2023.106845>
- CHASE, M.W. (1998) *NIST-JANAF Thermochemical Tables*. Fourth Edition, American Chemical Society, Washington, D.C.
- COOGAN, L.A., SEYFRIED, W.E., PESTER, N.J. (2019) Environmental controls on mid-ocean ridge hydrothermal fluxes. *Chemical Geology* 528, 119285. <https://doi.org/10.1016/j.chemgeo.2019.119285>
- CORRE, M., BRUNET, F., SCHWARTZ, S., GAUTHERON, C., AGRANIER, A., LESIMPLE, S. (2023) Quaternary low-temperature serpentinization and carbonation in the New Caledonia ophiolite. *Scientific Reports* 13, 19413. <https://doi.org/10.1038/s41598-023-46691-y>
- DELACOUR, A., FRÜH-GREEN, G.L., FRANK, M., GUTJAHN, M., KELLEY, D.S. (2008) Sr- and Nd-isotope geochemistry of the Atlantis Massif (30°N, MAR): Implications for fluid fluxes and lithospheric heterogeneity. *Chemical Geology* 254, 19–35. <https://doi.org/10.1016/j.chemgeo.2008.05.018>
- DEWANDEL, B., LACHASSAGNE, P., BOUDIER, F., AL-HATTALI, S., LADOUCHÉ, B., PINAULT, J.-L., AL-SULEIMANI, Z. (2005) A conceptual hydrogeological model of ophiolite hard-rock aquifers in Oman based on a multiscale and a multi-disciplinary approach. *Hydrogeology Journal* 13, 708–726. <https://doi.org/10.1007/s10040-005-0449-2>
- ELLISON, E.T., TEMPLETON, A.S., ZEIGLER, S.D., MAYHEW, L.E., KELEMEN, P.B., MATTER, J.M., The Oman Drilling Project Science Party (2021) Low-Temperature Hydrogen Formation During Aqueous Alteration of Serpentinized Peridotite in the Samail Ophiolite. *Journal of Geophysical Research: Solid Earth* 126, e2021JB021981. <https://doi.org/10.1029/2021JB021981>
- FRÜH-GREEN, G.L., KELLEY, D.S., BERNASCONI, S.M., KARSON, J.A., LUDWIG, K.A., BUTTERFIELD, D.A., BOSCHI, C., PROSKUROWSKI, G. (2003) 30,000 Years of Hydrothermal Activity at the Lost City Vent Field. *Science* 301, 495–498. <https://doi.org/10.1126/science.1085582>
- JÖNS, N., KAHL, W.-A., BACH, W. (2017) Reaction-induced porosity and onset of low-temperature carbonation in abyssal peridotites: Insights from 3D high-resolution microtomography. *Lithos* 268–271, 274–284. <https://doi.org/10.1016/j.lithos.2016.11.014>
- KELEMEN, P.B., LEONG, J.A., DE OBESO, J.C., MATTER, J.M., ELLISON, E.T., TEMPLETON, A., NOTHAFT, D.B., ESLAMI, A., EVANS, K., GODARD, M., MALVOISIN, B., COGGON, J.A., WARSJ, N.H., PÉZARD, P., CHOE, S., TEAGLE, D.A.H., MICHIBAYASHI, K., TAKAZAWA, E., AL SULAIMANI, Z., The Oman Drilling Project Science Team (2021) Initial Results From the Oman Drilling Project Multi-Borehole Observatory: Petrogenesis and Ongoing Alteration of Mantle Peridotite in the Weathering Horizon. *Journal of Geophysical Research: Solid Earth* 126, e2021JB022729. <https://doi.org/10.1029/2021JB022729>



- KLEIN, F., HUMPHRIS, S.E., BACH, W. (2020) Brucite formation and dissolution in oceanic serpentinite. *Geochemical Perspectives Letters* 16, 1–5. <https://doi.org/10.7185/geochemlet.2035>
- LASAGA, A.C. (1998) *Kinetic Theory in the Earth Sciences*. Princeton University Press, Princeton, NJ.
- LEONG, J.A., NIELSEN, M., MCQUEEN, N., KAROLYI, R., HILLEGONDS, D.J., BALLENTINE, C., DARRAH, T., MCGILLIS, W., KELEMEN, P. (2023) H₂ and CH₄ outgassing rates in the Samail ophiolite, Oman: Implications for low-temperature, continental serpentinization rates. *Geochimica et Cosmochimica Acta* 347, 1–15. <https://doi.org/10.1016/j.gca.2023.02.008>
- LOUTHAN JR., M.R., DERRICK, R.G. (1975) Hydrogen transport in austenitic stainless steel. *Corrosion Science* 15, 565–577. [https://doi.org/10.1016/0010-938X\(75\)90022-0](https://doi.org/10.1016/0010-938X(75)90022-0)
- MALVOISIN, B., BRUNET, F., CARLUT, J., MONTES-HERNANDEZ, G., FINDLING, N., LANSON, M., VIDAL, O., BOTTERO, J.-Y., GOFFÉ, B. (2013) High-purity hydrogen gas from the reaction between BOF steel slag and water in the 473–673 K range. *International Journal of Hydrogen Energy* 38, 7382–7393. <https://doi.org/10.1016/j.ijhydene.2013.03.163>
- MALVOISIN, B., BRANTUT, N., KACZMAREK, M.-A. (2017) Control of serpentinisation rate by reaction-induced cracking. *Earth and Planetary Science Letters* 476, 143–152. <https://doi.org/10.1016/j.epsl.2017.07.042>
- MALVOISIN, B., ZHANG, C., MÜNTENER, O., BAUMGARTNER, L.P., KELEMEN, P.B., Oman Drilling Project Science Party (2020) Measurement of Volume Change and Mass Transfer During Serpentinization: Insights From the Oman Drilling Project. *Journal of Geophysical Research: Solid Earth* 125, e2019JB018877. <https://doi.org/10.1029/2019JB018877>
- MALVOISIN, B., AUZENDE, A.-L., KELEMEN, P.B., the Oman Drilling Project Science Party (2021) Nanostructure of serpentinisation products: Importance for water transport and low-temperature alteration. *Earth and Planetary Science Letters* 576, 117212. <https://doi.org/10.1016/j.epsl.2021.117212>
- MCCOLLOM, T.M., BACH, W. (2009) Thermodynamic constraints on hydrogen generation during serpentinization of ultramafic rocks. *Geochimica et Cosmochimica Acta* 73, 856–875. <https://doi.org/10.1016/j.gca.2008.10.032>
- MCCOLLOM, T.M., DONALDSON, C. (2016) Generation of Hydrogen and Methane during Experimental Low-Temperature Reaction of Ultramafic Rocks with Water. *Astrobiology* 16, 389–406. <https://doi.org/10.1089/ast.2015.1382>
- MCCOLLOM, T.M., KLEIN, F., ROBBINS, M., MOSKOWITZ, B., BERQUÓ, T.S., JÖNS, N., BACH, W., TEMPLETON, A. (2016) Temperature trends for reaction rates, hydrogen generation, and partitioning of iron during experimental serpentinization of olivine. *Geochimica et Cosmochimica Acta* 181, 175–200. <https://doi.org/10.1016/j.gca.2016.03.002>
- MILLER, H.M., MAYHEW, L.E., ELLISON, E.T., KELEMEN, P., KUBO, M., TEMPLETON, A.S. (2017) Low temperature hydrogen production during experimental hydration of partially-serpentinized dunite. *Geochimica et Cosmochimica Acta* 209, 161–183. <https://doi.org/10.1016/j.gca.2017.04.022>
- MOODY, J.B. (1976) Serpentinization: a review. *Lithos* 9, 125–138. [https://doi.org/10.1016/0024-4937\(76\)90030-X](https://doi.org/10.1016/0024-4937(76)90030-X)
- NEAL, C., STANGER, G. (1983) Hydrogen generation from mantle source rocks in Oman. *Earth and Planetary Science Letters* 66, 315–320. [https://doi.org/10.1016/0012-821X\(83\)90144-9](https://doi.org/10.1016/0012-821X(83)90144-9)
- NEUBECK, A., DUC, N.T., HELLEVANG, H., OZE, C., BASTVIKEN, D., BACSIK, Z., HOLM, N.G. (2014) Olivine alteration and H₂ production in carbonate-rich, low temperature aqueous environments. *Planetary and Space Science* 96, 51–61. <https://doi.org/10.1016/j.pss.2014.02.014>
- PARKHURST, D.L., APPELO, C.A.J. (2013) *Description of Input and Examples for PHREEQC Version 3—A Computer Program for Speciation, Batch-Reaction, One-Dimensional Transport, and Inverse Geochemical Calculations*. USGS Techniques and Methods 6–A43, U.S. Geological Survey, Denver, CO. <https://pubs.usgs.gov/tm/06/a43/>
- SNOW, J.E., REISBERG, L. (1995) Os isotopic systematics of the MORB mantle: results from altered abyssal peridotites. *Earth and Planetary Science Letters* 133, 411–421. [https://doi.org/10.1016/0012-821X\(95\)00099-X](https://doi.org/10.1016/0012-821X(95)00099-X)
- ZIEMNIAK, S.E., JONES, M.E., COMBS, K.E.S. (1995) Magnetite solubility and phase stability in alkaline media at elevated temperatures. *Journal of Solution Chemistry* 24, 837–877. <https://doi.org/10.1007/BF00973442>

